Barrier layers and tropical Atlantic SST biases in coupled GCMs.

W.-P. Breugem[1], P. Chang[2], C. J. Jang[2,3], J. Mignot[4] & W. Hazeleger[1]

Submitted to Tellus A, September 13, 2007

[1] Royal Netherlands Meteorological Institute (KNMI), De Bilt, The Netherlands
[2] Department of Oceanography, Texas A&M University, College Station, Texas, USA
[3] Korea Ocean Research & Development Institute (KORDI), Ansan, Rep. of Korea
[4] LOCEAN, Université Pierre et Marie Curie, Paris, France

Abstract

The Northwestern Tropical Atlantic (NwTA) is one of the regions in the tropical oceans where thick barrier layers (BLs) form during boreal fall and winter. Once formed, BLs tend to inhibit entrainment cooling of the mixed layer. Compared to observations, many coupled General Circulation Models (GCMs) misrepresent the dynamics of BLs. It is shown that this may contribute to the cold Sea Surface Temperature (SST) bias over the NwTA, which causes the Intertropical Convergence Zone (ITCZ) to migrate too far southward in the models. On the other hand, many models simulate spurious BLs in the Southeastern Equatorial Atlantic (SeEA). These BLs contribute to the warm SST bias over this region. They originate partly from overestimated precipitation associated with the displaced ITCZ and partly from a subsurface warm bias associated with the underestimated equatorial trades during boreal spring and summer. However, it is difficult to separate cause and effect of the biases because of strong air-sea coupling in the tropics. Potential ocean-atmosphere feedback mechanisms involving BL-SST-ITCZ interactions are presented. An implication of our study is that the upper ocean salinity stratification in coupled GCMs need to be improved, as it may play an important role in maintaining the tropical Atlantic climate.

1 Introduction

The ocean surface mixed–layer is the turbulent surface layer of the ocean with a vertically uniform density, temperature and salinity distribution. In the tropics, the base of the mixed layer corresponds to the top of the pycnocline. Over most of the tropical oceans the pycnocline coincides with the thermocline, but in regions with a strong vertical salinity stratification the pycnocline can be shallower than the thermocline. In this case, the layer

between the top of the pycnocline and the top of the thermocline is called 'barrier layer' (Godfrey & Lindstrom, 1989; Sprintall & Tomczak, 1992), because it forms a barrier to entrainment and turbulent mixing of cold thermocline water into the mixed layer and inhibits the downward mixing of momentum (e.g. Vialard & Delecluse, 1998a). BLs thus have an impact on the SST and the surface currents (Murtugudde & Busalacchi, 1998; Maes et al., 2002).

Observational studies show that BLs can occur over the western and equatorial tropical Atlantic (Sprintall & Tomczak, 1992; Pailler et al., 1999; Foltz et al., 2004; Sato et al., 2006; de Boyer Montégut et al., 2007; Mignot et al., 2007). Advection of fresh water from the Amazon river by surface currents along the northern coast of South America induces thick BLs in this area in boreal winter and spring (Pailler et al., 1999, Masson & Delecluse, 2001). In summer, the North Equatorial Counter Current (NECC) carries part of the fresh Amazon water eastward across the basin, which reinforces the BLs induced by intense local precipitation in the ITCZ (e.g. Pailler et al., 1999). The tropical Atlantic is also characterized by robust BLs located equatorward of the subtropical salinity maxima during the winter season of both hemispheres. Their formation mechanism is still under debate (Sato et al., 2006; Mignot et al., 2007). In a recent study of in situ measurements at (38°W,15°N), Foltz & McPhaden (2007) show that the BLs at this location play a considerable, though secondary, role in modulating the seasonal cycle of the SST by suppressing entrainment cooling of the mixed layer during boreal winter. Finally, Mignot et al. (2007) underlined the presence of up to ~ 50 m thick BLs east of the Caribbean basin and north of South America in boreal fall and winter. These BLs are characterized by a subsurface temperature inversion of which the maximum temperature is typically $\sim 0.5 - 0.6$°C higher than the mixed–layer temperature (de Boyer Montégut et al., 2007). They are probably formed by advection of fresh water from the Amazon river by surface currents in combination with surface cooling during boreal fall and winter (Mignot et al., 2007).

Many of the modeling studies on BL dynamics have been focused on the warm pool region in the western Pacific (e.g. Vialard & Delecluse, 1998a,1998b; Maes et al., 2002). Masson & Delecluse (2001) were the first to use an ocean GCM to study the formation of BLs in the Atlantic warm pool region. The use of an ocean–only model excludes interactions between the ocean and the atmosphere, which are known to be strong in the tropics, making it difficult to address issues concerning the climatic impact of BLs (Murtugudde & Busalacchi, 1998; Maes et al., 2002). The present study attempts to investigate the climatic circumstances and impact of BLs in the tropical Atlantic by analyzing fully coupled ocean–atmosphere GCM simulations.

Breugem et al. (2006) recently diagnosed systematic biases of nine coupled GCMs in simulating the tropical Atlantic climate. Biases that are common to all the models include a warm SST bias over the SeEA, especially in boreal summer, and a cold SST bias over the NwTA. As a result, in boreal summer the zonal SST gradient along the equator is directed toward the west in the models instead of toward the east in the observations. In the same season, the simulated easterly trade winds along the equator are too weak. Similar biases were reported on the previous generation of coupled models (Davey et al., 2002). Furthermore, the simulated marine ITCZ with the associated band of deep convection and

Model (run #)	period	Res. Atm.	Res. Ocean	Reference
CNRM-CM3 (1)	1900-1929	T63L45	2° x 0.5° L31	(Salas-Mélia et al., 2005)
CSIRO-Mk3.0 (2)	1901-1930	T63L18	1.875° x 0.84° L31	(Gordon et al., 2002)
UKMO-HadCM3 (2)	1900-1924	3.75° x 2.5° L19	1.25° x 1.25° L20	(Gordon et al., 2000)

Table 1: Coupled ocean–atmosphere models considered in this study, with the run number of the 20th–century–climate (20c3m) scenario between brackets. The ocean resolution is given along the equator.

intense precipitation migrates too far southward into the southern hemisphere — a bias that is also typical for atmospheric GCMs forced with observed SST (Biasutti et al., 2006).

One of the particularly pronounced characteristics of the models is the failure to accurately simulate the development of the equatorial Atlantic Cold Tongue (ACT) when the SST in the SeEA drops by about 6°C from late boreal spring to summer. In reality, the ACT develops as a result of increased entrainment and turbulent mixing of cold subsurface water into the mixed layer (Foltz et al., 2003). These processes are associated with the onset of the West African monsoon in May–June with the intensification of southerlies across the equator in the east (Philander & Pacanowski, 1981) and enhanced easterlies further to the west (Mitchell & Wallace, 1992; Okumura & Xie, 2004). The low SST and the cross–equatorial southerlies prevent the migration of the ITCZ into the southern hemisphere. Positive ocean–atmosphere feedbacks tend to maintain the cold tongue and the northerly position of the ITCZ (Mitchell & Wallace, 1992; Chang & Philander, 1994; Okumura & Xie, 2004; Xie, 2004, and references therein).

The aim of this study is to examine the ability of fully coupled GCMs to simulate BLs in the tropical Atlantic and to assess the extent to which SST biases can be attributed to errors in the simulated BLs. The paper is organized as follows. Section 2 gives an overview of the models and data used in this study. Section 3 is concerned with the definition of a BL. The BL characteristics of the models are presented in section 4. The mechanisms behind spurious model BLs in the SeEA is further discussed in 5. Section 6 is dedicated to model biases in the SST and the surface wind stress. In section 7 the contribution of BLs to SST biases is explored. This is followed by a discussion in section 8. Finally, the main conclusions are given in section 9.

2 Models and data

Table 1 lists the fully coupled GCMs that are analyzed in the present study. The models are selected, based on the availability of subsurface ocean data, from the list of coupled GCMs used for the fourth assessment report of the Intergovernmental Panel on Climate Change (IPCC, 2007). For the analysis we made use of monthly mean model output of the period 1900-1930 of the 20th–century–climate (20c3m) scenario simulations.

To assess model biases, the model output for the ocean is compared against the 1972-2001 period of the Simple Ocean Data Assimilation (SODA) reanalysis (version 1.4.2;

Carton & Giese, 2007). Biases in SST and surface wind stress are computed as the differences in reference to the ERA-40 reanalysis for 1958-2001. Rainfall biases are computed with respect to the CMAP precipitation data (Xie & Arkin, 1997) for 1979-2005 provided by NOAA/OAR/ESRL PSD, Boulder, Colorado, USA, from their web site at http://www.cdc.noaa.gov/.

3 Definition of BLs

Following de Boyer Montégut et al. (2004) and Mignot et al. (2007), we define the top of the thermocline, or equivalently the isothermal layer depth (ILD), as the depth where the potential temperature has dropped by 0.2°C with respect to its value at 10 m. Similarly, the top of the pycnocline, which corresponds to the mixed–layer depth (MLD), is defined as the depth where the potential density has increased with respect to its value at 10 m by an amount that corresponds to a drop in potential temperature by 0.2°C. In mathematical form, the above definitions can be expressed as:

$$\theta_{\mathrm{z=-ILD}} \equiv \theta_{\mathrm{10m}} - 0.2, \tag{1}$$

$$\sigma_{\mathrm{z=-MLD}} \equiv \sigma(S_{\mathrm{10m}}, \theta_{\mathrm{10m}} - 0.2), \tag{2}$$

where θ is the potential temperature, S is the salinity, and σ is the potential density. In this study the potential density is computed from the 1980 UNESCO International Equation of State (IES80; Gill, 1982). The reference depth of 10 m is based on avoiding the diurnal variability in the vertical stratification in the top few meters just below the ocean surface. Note that the above definitions imply that the ILD and MLD are at least 10 m thick.

Over most of the tropical Atlantic the pycnocline coincides with the thermocline. An example of this is illustrated in figure 1.a, which shows the vertical stratification of density, salinity and potential temperature at (30°W,25°N) in January 1978 according to SODA. Within the mixed layer, which is approximately 70 m thick at this site and time, the profiles are uniform. Just below the mixed layer, the temperature rapidly decreases, while the density increases with depth.

Figure 1.b shows the stratification at a different site (50°W,15°N) in the same month. At this location, the vertical salinity stratification is much stronger than at (30°W,25°N). As a consequence, the mixed layer is about 2.5 times shallower than the isothermal layer. A 40 m thick BL exists between the bottom of the isothermal layer and the mixed layer. The strong salinity stratification even enables a stable density stratification with a temperature inversion inside the BL, that is, the maximum temperature occurs below the mixed layer and it is about 0.3°C higher than the temperature within the mixed layer. Note that when this occurs, entrainment and vertical turbulent mixing at the base of the mixed layer tend to warm the mixed layer contrary to a cooling tendency in the case shown in figure 1.a.

The strong salinity stratification in figure 1.b traps the net surface cooling during boreal fall and winter in the mixed layer. Simultaneously, a part of the surface solar radiation penetrates below the mixed layer and tends to heat up the BL (Vialard & Delecluse, 1998a;

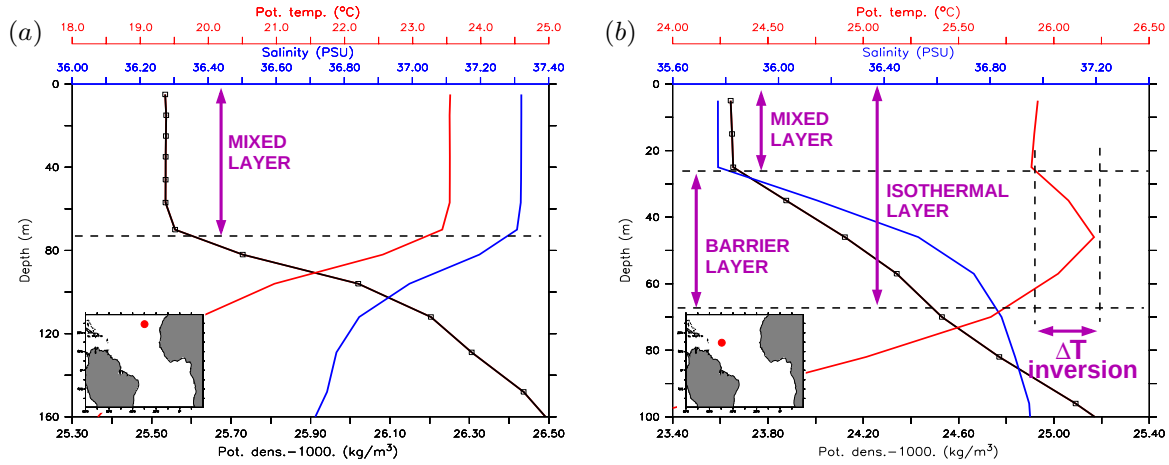

Figure 1: Examples of vertical stratifications in the tropical Atlantic ocean (a) without and (b) with a BL. The profiles were taken from SODA, January 1978, at the location of the red dot in the insert (30°W,25°N and 50°W,15°N, respectively). The black, red and blue lines depict, respectively, the potential density (in kg/m^3), the potential temperature (in °C), and the salinity (in PSU). The square symbols indicate the vertical grid resolution of the data.

Masson & Delecluse, 2001). These processes may explain the existence of the temperature inversion in figure 1.b.

4 BL characteristics

In this section some BL characteristics of the models are shown and compared against the SODA reanalysis for both boreal winter and summer. The detailed procedure for computing these characteristics is given in the appendix.

4.1 Boreal winter

Figure 2 shows the frequency of BL occurrence, the BL thickness and the magnitude of temperature inversions for boreal winter. The results from SODA are shown in the far left column and the model results are depicted in the three right columns. The SODA climatology for the BL thickness (figure 2.a) agrees fairly well with figures 1 and 5 in Mignot et al. (2007) derived from the NODC, WOCE and ARGO databases of measured salinity and temperature profiles. The common features are a vast area of thick BLs of up to $\sim$ 40 m east of the Caribbean basin and north of South America (box 1) and further south along the northern coast of South America, BLs equatorward of the northern subtropical salinity maximum (box 2), and thinner BLs of $\sim$ 15 m near 5°N and west of 20°W (box

3). However, the BLs equatorward of the southern subtropical salinity maximum around $\sim 10°$S (box 4) do not appear in this season in the observations. Furthermore, SODA also exhibits unrealistic occasional BLs directly off the coast of Northwest Africa near 20°N.

The models reproduce the presence of thick BLs east of the Caribbean basin and north of South America in boreal winter, but they underestimate the regional extent of the BLs. Furthermore, the thickness of the BLs and their frequency of occurrence are generally underestimated, with the notable exception of a small core region centered around $\sim$ (60°W,18°N) in the CSIRO-Mk3.0, where the BLs are too thick and too frequent (figures 2.c,g). Both SODA and the models show that the thick BLs in this region are accompanied with a temperature inversion. The maximum temperature inversion in SODA is of the order of 0.5°C, in agreement with the observational results of de Boyer Montégut et al. (2007), while in the CSIRO-Mk3.0 and the UKMO-HadCM3 model it is roughly twice too strong.

As mentioned in the introduction, the thick BLs with temperature inversions are believed to originate primarily from advection of fresh Amazon water by surface ocean currents in combination with surface cooling during boreal fall and winter (Mignot et al., 2007). This mechanism seems to be consistent with the Sea Surface Salinity (SSS) field of SODA (not shown), which clearly shows a low salinity plume extending from the mouth of the Amazon river ($\sim$ 50°W,0°N) along the northern coast of South America toward the east of the Caribbean basin. A similar plume is visible in the BL characteristics of SODA (figures 2.a,e,i). The BL characteristics of the models also exhibit plume–like features, although less pronounced compared to SODA.

The underestimation of the regional extent of BLs over the NwTA in the models is likely related to the SSS bias in this region. In particular, during boreal fall, the SSS near the Amazon river mouth is too high in the models compared to SODA (not shown), suggesting that the Amazon river discharge is underestimated. This is further discussed in section 8.

4.2 Boreal summer

Figure 3 shows the BL characteristics for boreal summer. Again the SODA climatology for the BL thickness (figure 3.a) agrees reasonably well with the observational results shown in figures 1 and 5 in Mignot et al. (2007). Both SODA and the observations show the existence of BLs east of the Caribbean basin and north of South America (box 1), but with a smaller regional extent and less thick than in winter, and both show that the BL region south of the northern subtropical salinity maximum (box 2) has vanished (figure 3.e). Both also exhibit a BL region around 5°N (box 3), though it appears more pronounced in the observations than in SODA. Furthermore, both show the presence of BLs equatorward of the southern subtropical salinity maximum around $\sim 10°$S (box 4), but with a substantially smaller regional extent and less thick BLs in the observations than in SODA.

The models capture the reduction in the extent and the thickness of the BLs east of the Caribbean basin in boreal summer (boxes 1 and 2), presumably as a result of summer warming and a reduction in wind–induced mixing (Mignot et al., 2007). However, the differences among the models are large. The BL thickness and in particular the frequency

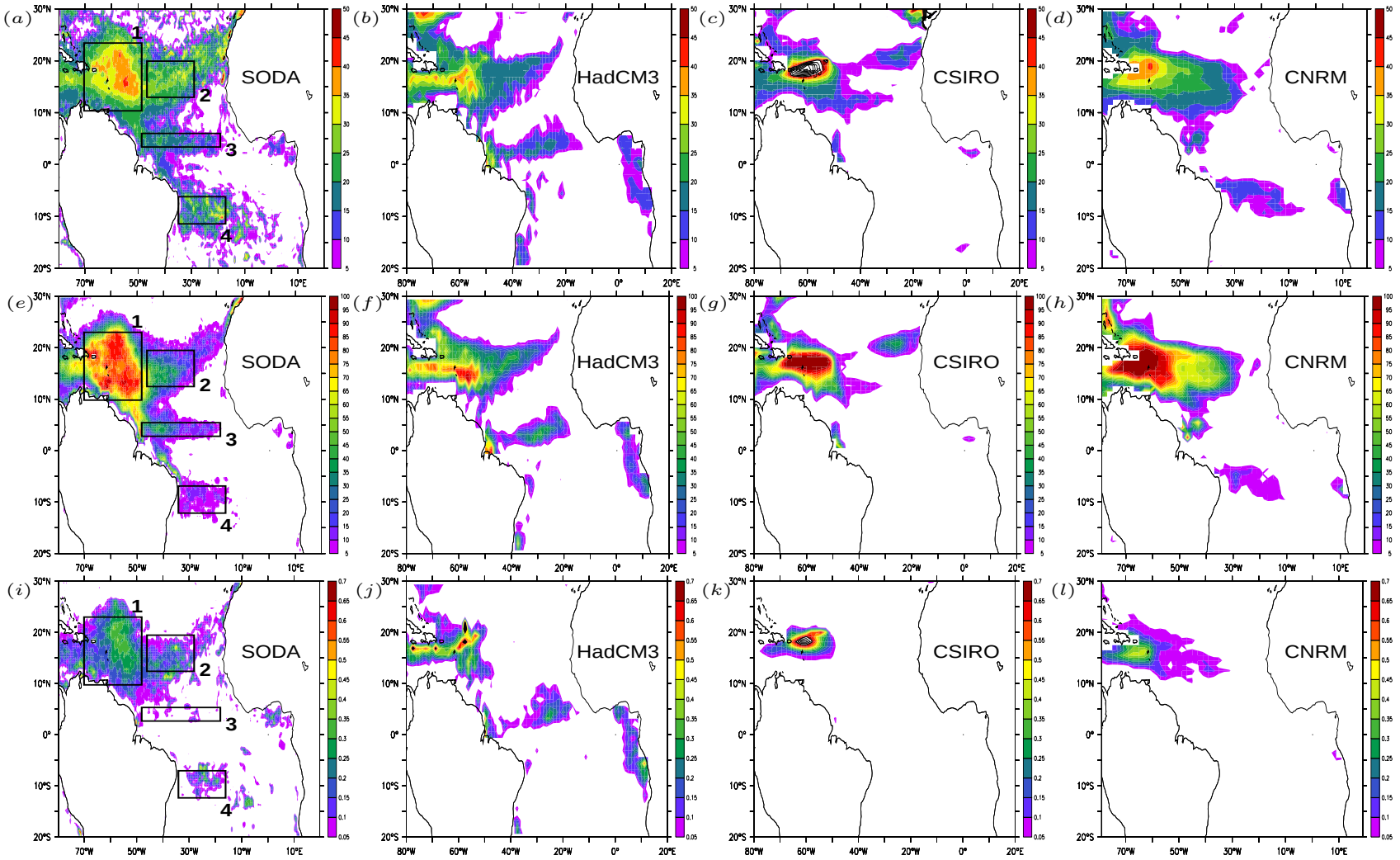

Figure 2: BL characteristics averaged over boreal winter (DJF) in SODA (far left column) and in the models (three right columns). See the appendix for definitions. Values beyond the range of the colorkey have been contoured; the contour interval is equal to the color interval. (a)-(d) BL thickness (in m). (e)-(h) Frequency of BL occurrence (in %). (i)-(l) Magnitude of temperature inversion (in °C).

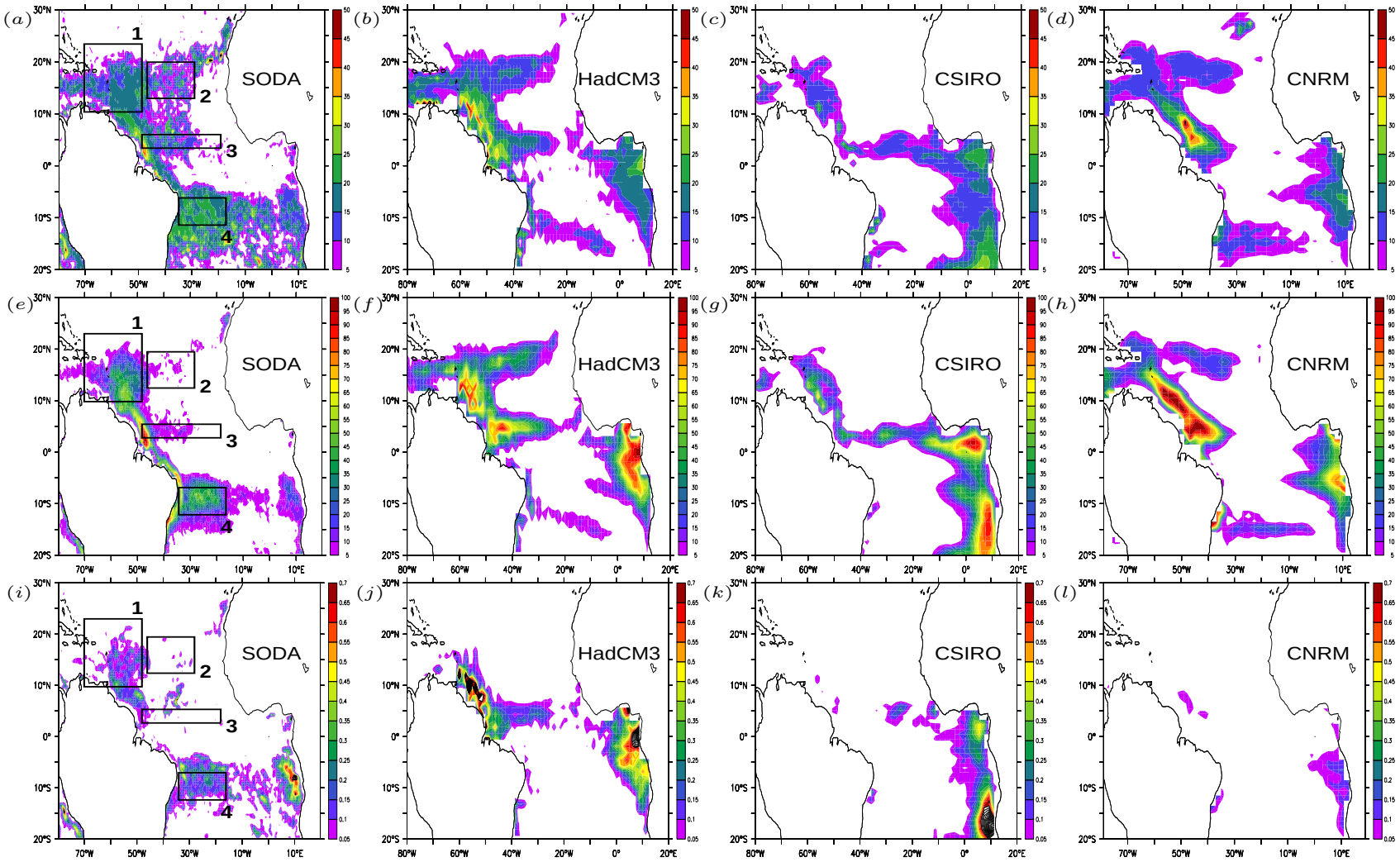

Figure 3: Idem as for figure 2, but now for boreal summer (JJA).

of BL occurrence in this region are largely overestimated by the UKMO-HadCM3 model, while underestimated by the CSIRO-Mk3.0 model. Furthermore, temperature inversions in this BL region occur only in the UKMO-HadCM3 model.

All models capture the BL region around 5°N, although again large differences are seen among the models and between the models and SODA. In reality the fresh surface water of this BL region originates partly from the Amazon river, which feeds the North Brazil Current (NBC). A part of the water from the NBC flows into the NBC retroflection and is advected eastward by the NECC along $\sim 6°$N during boreal summer and fall (e.g. Pailler et al., 1999; Mignot et al., 2007). This mechanism is likely to play an important role in the formation of these BLs in the UKMO-HadCM3 model, as figures 3.b,f,j clearly show a plume from the mouth of the Amazon river, extending northward along the western boundary and then eastward along the NECC. Intense local precipitation associated with the overlying ITCZ may also have contributed to the formation of the BLs (Foltz et al., 2004; Mignot et al., 2007).

The models poorly simulate the BL region off the Brazil coast around $\sim 10°$S (box 4). It has been suggested by Mignot et al. (2007) that the formation of these BLs is linked to the presence of salty subsurface water subducted from the southern subtropical SSS maximum just poleward of this BL region. In the models the southern subtropical SSS maximum is too low by more than 1 PSU (not shown), which is consistent with the absence of this BL region in the models.

Another striking difference between the models and SODA/observations is that the models appear to simulate spurious BLs over the SeEA off the African coast. Locally the frequency of occurrence can reach values of up to 100 %. Temperature inversions also display very high values, with maxima larger than 1°C for the UKMO-HadCM3 and the CSIRO-Mk3.0 models. The thickness of these BLs is typically in the range of 10-20 m. Interestingly, this BL region coincides with the ACT region where the models show a strong warm SST bias as discussed in the introduction. The mechanisms behind the presence of this BL region in the models will be discussed in the next section.

5 Mechanisms of spurious model BLs in the SeEA

Figure 4 presents the seasonal variation of the vertical stratification in salinity and temperature horizontally averaged over the ACT region. The latter is defined here as the region extending from 10°W to 10°E and 5°S to 0°N. The solid and dashed lines depict the seasonal cycle of the MLD and the ILD, respectively. In SODA, the MLD follows closely the ILD throughout the year, indicating that the vertical stratification in density is mainly controlled by the temperature. Indeed, the seasonal variation in the salinity stratification is weak, while it is strong in the temperature stratification (figures 4.a,b). The SST varies from near 29°C in March to 23.5°C in August. Similarly, the MLD and ILD vary between roughly 15 m in March and 20 m in October.

In contrast to SODA, for all three models the ILD is significantly larger than the MLD during boreal spring and summer. This indicates the presence of a BL in these seasons and

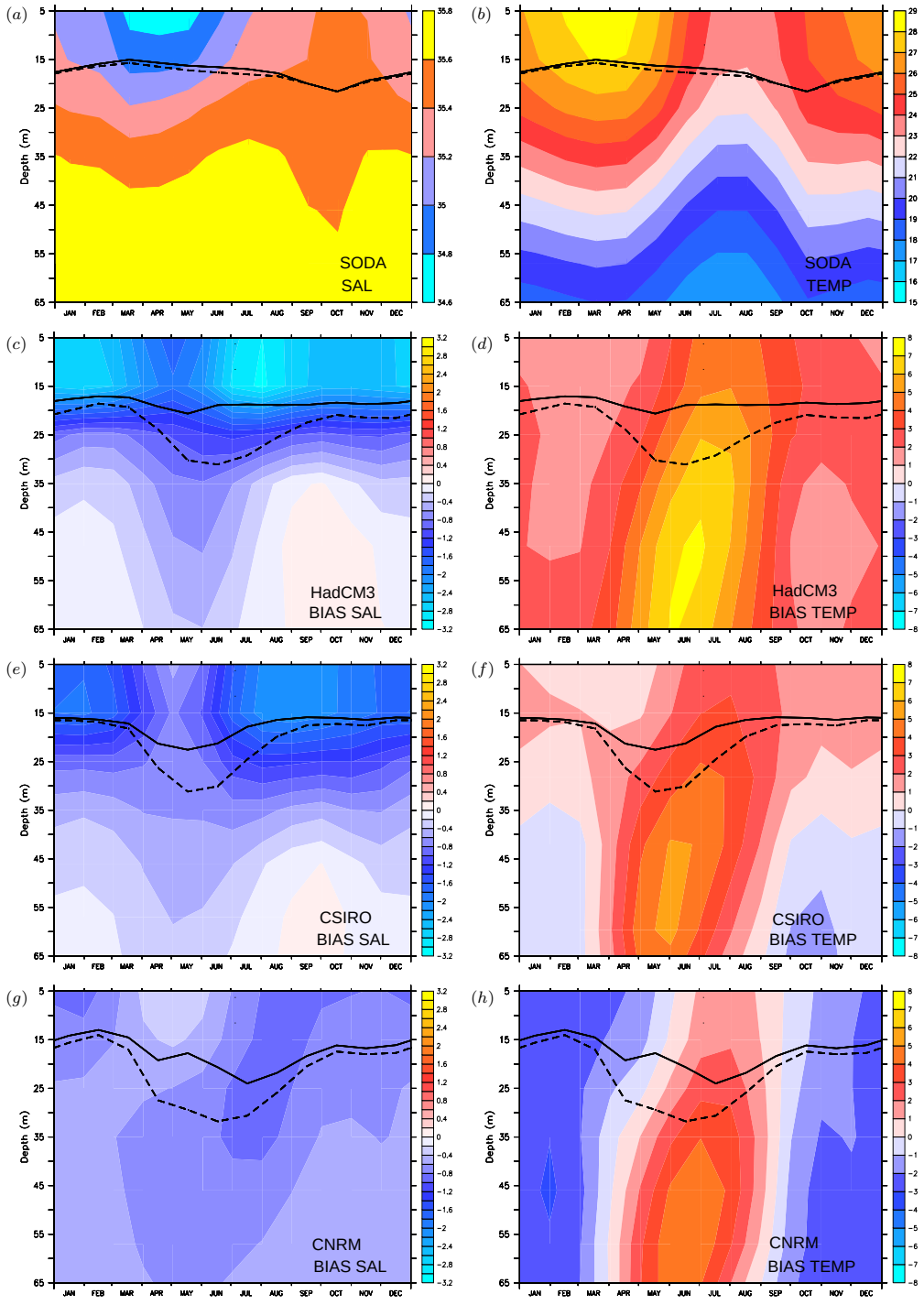

Figure 4: Vertical stratification in salinity (left panels, in PSU) and potential temperature (right panels, in °C) averaged over the ACT region from 10°W to 10°E and 5°S to 0°N. The solid and dashed lines depict, respectively, the mixed–layer depth and the isothermal layer depth. (a,b) SODA. (c,d) Biases UKMO-HadCM3 model. (e,f) Biases CSIRO-Mk3.0 model. (g,h) Biases CNRM-CM3 model.

hints at the important role of salinity in determining the vertical density stratification. In all models the isothermal layer deepens strongly from 15-20 m in boreal spring to about 30 m in early summer, while the variation in mixed–layer depth is much weaker. In the UKMO-HadCM3 model, the MLD remains nearly unchanged. The BL formation in the models, as revealed by figure 4, results from the combined effect of very fresh water at the surface and the development of a subsurface warm bias from spring to summer. These erroneous features are especially pronounced for the UKMO-HadCM3 model where the error in SSS is as large as 3 PSU (figure 4.c) and in temperature near 8°C at 45-65 m depth in June (figure 4.d).

The origin of the warm bias in the subsurface temperature will be discussed in the following section. Here we note that the temperature bias patterns of the models are tilted upward in the depth-time plots shown in figure 4, indicating that the subsurface temperature errors are 'propagating' upward into the mixed layer. While in SODA the upwelling of cold subsurface water in boreal spring and summer causes rapid cooling of the surface and the development of the ACT, in the models the subsurface warm bias substantially reduces the surface cooling. This thus may well explain the upward propagation of temperature biases.

Different from the temperature bias patterns, the salinity bias patterns of the models do not show an upward tilt, suggesting that the low salinity bias at the surface may be a consequence of horizonal advection by the surface currents and/or a local E-P surface flux error rather than related to subsurface processes. Figure 5 shows the model precipitation biases in the tropical Atlantic during JJA in reference to the CMAP observational dataset. The observations show that the position of the marine ITCZ is centered around the latitude band of 6-8°N. In the models the marine ITCZ is shifted toward the southeast, causing a negative precipitation bias to the north and a positive precipitation bias in and south of the ACT region. This suggests that the low SSS in the ACT region is caused by excessive rainfall. A budget analysis of the mixed–layer salinity confirmed that this is the primary cause of the low SSS, but also indicated an important contribution from meridional transport of fresh water by the surface currents (not shown). It is noted, however, that the latter contribution may actually also be related to excessive precipitation, since figure 5 shows that the precipitation bias pattern extends over the region just south of the ACT region.

6 SST and wind stress biases

In this section we discuss the model biases in SST and wind stress over the tropical Atlantic. The biases for DJF and JJA are depicted in figure 6. Note that for all models the SST bias patterns look fairly similar, which suggests that the SST biases may be caused by common physical processes. Cold SST biases are observed over the western equatorial Atlantic and further poleward of the equator. The wind stress bias of the CNRM-CM3 model (figure 6.c,f) shows that the trade wind over the northern tropical Atlantic is far too strong, suggesting that the strong cold SST bias of more than 3°C over this area may

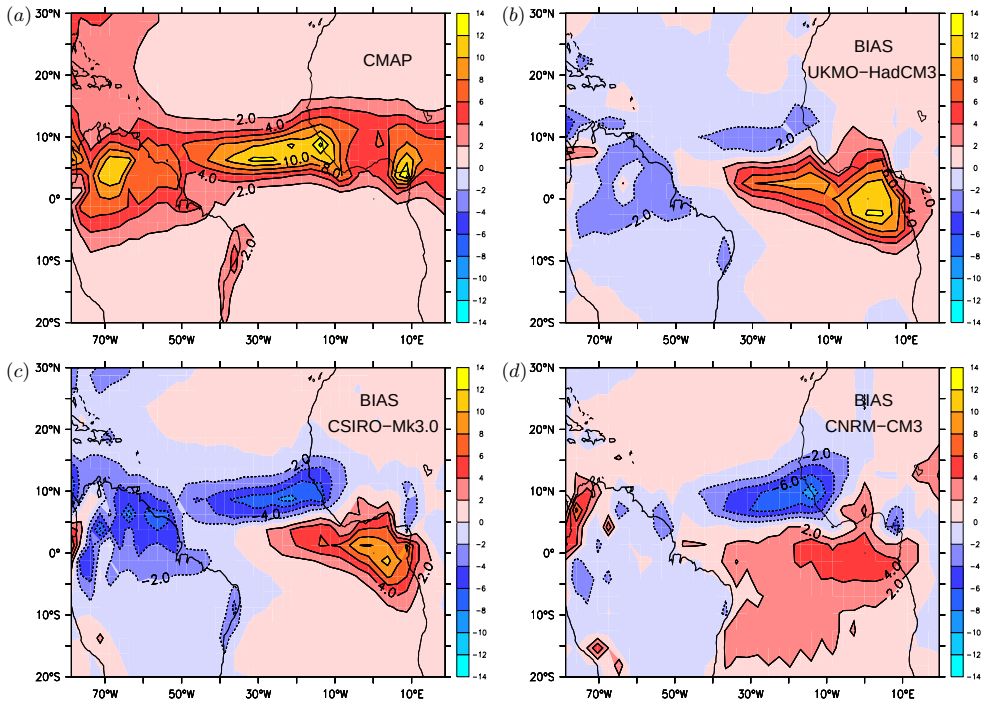

Figure 5: Rainfall in the tropical Atlantic during JJA (in mm/day). (a) CMAP observations. (b) Bias UKMO-HadCM3 model. (c) Bias CSIRO-Mk3.0 model. (d) Bias CNRM-CM3 model.

originate largely from excessive latent cooling. In contrast, the northeasterly trade wind is too weak in the UKMO-HadCM3 model, but this model still has a cold SST bias in this region, albeit weaker compared to the CNRM-CM3 model. This suggests that other physical processes also contribute to the cold bias. We will show in the following section that one of the physical factors may be related to the underestimation of the regional extent of BLs east of the Caribbean basin during DJF in the models (figure 2). The other region where a cold SST bias commonly appears in the models is the southwestern tropical Atlantic, which also appears to be a region where the models fail to simulate the formation of BLs during boreal summer (figure 3).

In all the models warm SST biases are observed over the SeEA in boreal summer, particularly in the UKMO-HadCM3 model with biases exceeding 5°C over the ACT region. As a consequence, the zonal SST gradient along the equator is directed toward the west in the models instead of toward the east in reality as depicted in figure 7.a. Consistent with the wrong zonal SST gradient and the accompanying bias in the zonal surface pressure gradient (not shown), there is a strong westerly wind bias in the equatorial trade. The westerly wind bias affects the depth of the thermocline as shown in figure 7.b. In the SODA reanalysis the thermocline is deeper than 125 m in the western equatorial Atlantic and shoals eastward to about 35 m. In the models, however, the thermocline is too shallow

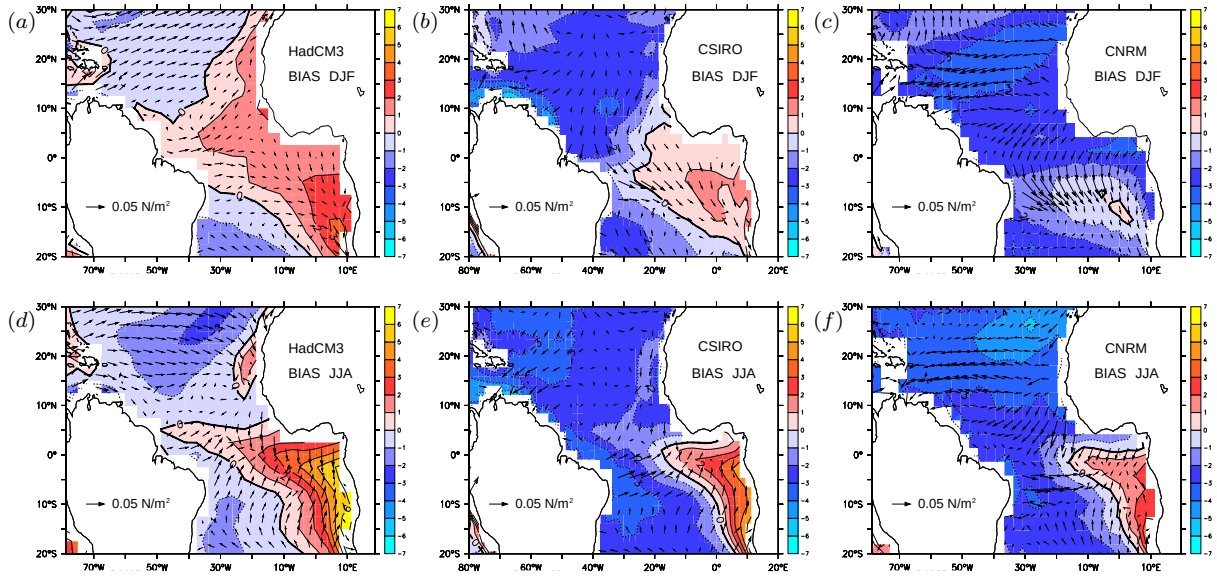

Figure 6: Model biases in SST and surface wind stress during DJF (top panels) and JJA (bottom panels) with respect to the ERA-40 reanalysis. (a,d) Biases UKMO-HadCM3 model. (b,e) Biases CSIRO-Mk3.0 model. (c,f) Biases CNRM-CM3 model.

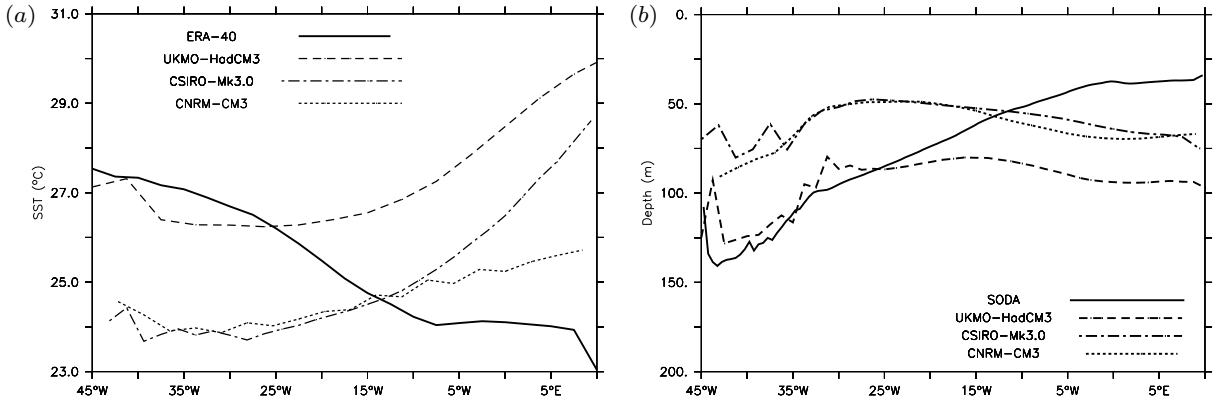

Figure 7: (a) Boreal summer (JJA) SST along the equator and averaged from 5°S till 0°N. Solid line represents the ERA-40 SST, while the other lines depict the SST for the models. (b) Idem for the depth of the 20°C-isotherm, which is a proxy for the depth of the equatorial thermocline.

in the west, but too deep in the east, and it reaches a minimum depth around 35-15°W.

The westerly wind bias and the associated thermocline bias over the eastern equatorial Atlantic, explain the strong warm subsurface temperature bias during spring and summer in figures 4.d,f,h. Furthermore, the cold SST bias over the northern tropical Atlantic and the strong warm SST bias over the SeEA are consistent with the southeastward displacement of the marine ITCZ in the models (figure 5), as deep convection tends to be collocated with the maxima in SST. One may therefore tend to attribute the fresh SSS bias over the SeEA to the warm SST bias. However, cause and effect are difficult to separate here, because the fresh SSS bias together with the warm subsurface temperature bias give rise to spurious BLs during boreal spring and summer (figure 4), which in turn affect the SST by suppressing entrainment and turbulent mixing of cold subsurface water into the mixed layer.

7 Contribution of BLs to SST biases

In previous sections we showed that there are two regions in the tropical Atlantic where the models display major biases in the representation of BLs. On the one hand, they develop spurious BLs with strong temperature inversions in the SeEA during boreal spring and summer (figures 3,4). On the other hand, they underestimate the regional extent and the frequency of occurrence of BLs in the NwTA during boreal fall and winter (figure 2). It may be expected that the BL biases contribute to the biases in the SST, since BLs affect the turbulent mixing and entrainment of cold subsurface water into the mixed layer. In this section this is investigated in more detail for the two mentioned BL regions. Although important, we are unable to give a direct assessment of biases in turbulent mixing, since this is parameterized in the models and difficult to reconstruct from the available model output. Instead, we analyzed the entrainment heat flux in the two BL regions.

The mixed–layer temperature tendency associated with the entrainment heat flux (EHF) through the base of the mixed layer can be written as (e.g. Stevenson & Niiler, 1983):

$$\left.\frac{\partial\langle T\rangle}{\partial t}\right|_{\mathrm{EHF}} = -\frac{\mathcal{H}(w_e)\, w_e\, \left[\langle T\rangle - T|_{-h}\right]}{h}, \tag{3}$$

where $\langle T\rangle \equiv (1/h)\int_{-h}^{0} T dz$ is the depth–averaged mixed–layer temperature, $w_e \equiv \partial h/\partial t + \nabla\cdot h\langle\mathbf{v}\rangle$ is the upward entrainment velocity through the base of the mixed layer that can be computed from the mixed–layer depth h and the horizontal velocity vector $\mathbf{v}$, and T_{-h} is the temperature at the base of the mixed layer. Following Kraus & Turner (1967), it is assumed that the mixed–layer temperature is only affected by entrainment when $w_e > 0$. Hence the inclusion of the Heaviside function, $\mathcal{H}(w_e)$, in equation (3), which is equal to 0 for $w_e < 0$, 1/2 for $w_e = 0$, and 1 for $w_e > 0$. The results for the entrainment heat flux shown in this section have been computed from the monthly mean output of the models and the SODA reanalysis. This implies that the estimate of the entrainment heat flux excludes the contribution from coupled variations in temperature and entrainment velocity on time

scales smaller than 1 month. Although this contribution might be significant, it could not be determined from the model output and therefore had to be ignored.

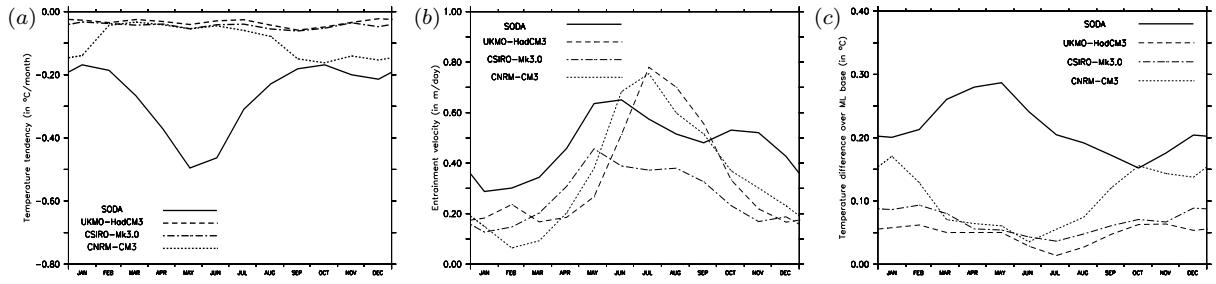

Figure 8: (a) Mixed–layer temperature tendency associated with the entrainment heat flux through the base of the mixed layer (in °C/month), averaged over the ACT region. (b) Upward entrainment velocity, $\mathcal{H}(w_e)\, w_e$ (in m/day). (c) Temperature difference over the base of the mixed layer in case of an upward entrainment velocity, $\mathcal{H}(w_e)\, [\langle T \rangle - T_{-h}]$ (in °C).

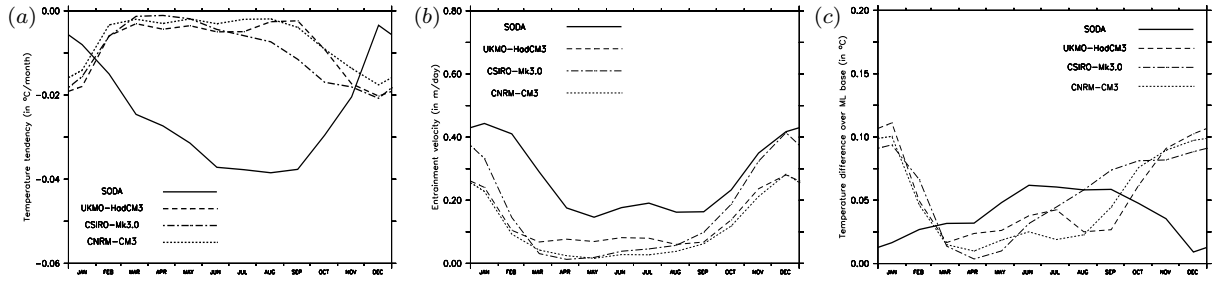

Figure 9: Idem as for figure 8, but now the quantities are averaged over the NwTA.

Figure 8.a depicts the entrainment–induced temperature tendency averaged over the ACT region for the models and the SODA reanalysis. The models strongly underestimate the entrainment cooling, in particular during late spring and early summer. During May–June the entrainment cooling varies between 0.03-0.06°C/month in the models, while it amounts to nearly 0.5°C/month in SODA. To investigate the cause of the underestimated entrainment cooling, the conditional climatologies (including only events with $w_e > 0$) of the entrainment velocity and the temperature difference over the base of the mixed layer are plotted in figures 8.b and 8.c, respectively. This shows that the bias in the entrainment heat flux can be mainly attributed to the strong underestimation of the temperature difference over the base of the mixed layer, in particular during boreal spring and summer. This in turn can be related to the presence of spurious BLs over the ACT region (figures 3,4).

Integrated over boreal spring and summer (March–August), the bias in the entrainment heat flux is responsible for an increase in the SST bias over the ACT region of 1.8-2°C in

all three models. Although smaller, these numbers are of the same order as the March–August increase in the warm SST bias shown in figures 4.d,f,h. Besides entrainment cooling, observational and modeling studies indicate that vertical turbulent mixing at the base of the mixed layer also contributes significantly to the development of the equatorial Atlantic cold tongue (Foltz et al., 2003; Jochum et al., 2005; Peter et al., 2006). Like entrainment, vertical turbulent mixing scales with the temperature difference over the mixed–layer base. It is therefore expected that the cooling associated with vertical turbulent mixing is also underestimated by the models, and this may thus have contributed to the warm SST bias as well.

Figure 9 shows the entrainment–induced temperature tendency averaged over the NwTA region, which is defined here as the region extending from 65°W to 45°W and 10°N to 25°N. The models underestimate the entrainment cooling from March–September, which seems to originate primarily from an underestimation of the entrainment velocity (figure 9.b). In contrast with this, the models overestimate entrainment cooling during November–January, which can be related to overestimation of the temperature difference over the mixed–layer base (figure 9.c). This is consistent with an underestimation of the regional extent and frequency of occurrence of BLs in the NwTA (figure 2).

The effect of the bias in entrainment heat flux on the SST over the NwTA seems to be small. The largest negative bias is found for December when it amounts to -0.03°C/month (figure 9.a). However, the models likely also overestimate cooling by vertical turbulent mixing. Biases in the formation of BLs over the NwTA may thus be responsible for a larger negative SST bias than estimated from the bias in entrainment cooling only.

8 Discussion

From the analysis presented in the previous section one might conclude that the systematic model biases in simulating BLs only have a significant impact on SST biases in the SeEA, while their impact is relatively small in the NwTA. However, this conclusion may be misleading because it does not fully take into account the consideration of coupled ocean–atmosphere feedbacks. The tropical Atlantic is an area where ocean–atmosphere interactions are known to be strong. Because of the active air–sea coupling, small model errors in one physical process can cause chain reactions and affect other physical processes. For example, BL biases can cause SST biases which in turn can affect atmospheric convection, introducing errors to surface heat fluxes and other physical processes. This makes it very difficult to pinpoint exactly how much of the model SST biases can be attributed to BL biases. Therefore, further understanding of the impact of BLs on SST requires the understanding of coupled feedbacks in the climate system. Some potential feedback mechanisms are illustrated in figure 10 and discussed below.

The lack of BLs over the NwTA during boreal fall and winter is responsible for excessive mixed–layer cooling by vertical entrainment and turbulent mixing, and partly contributes to the cold SST bias over this region. The cold SST bias tends to displace the ITCZ toward the southeast. Consequently, rainfall is reduced over the NwTA and the Amazon

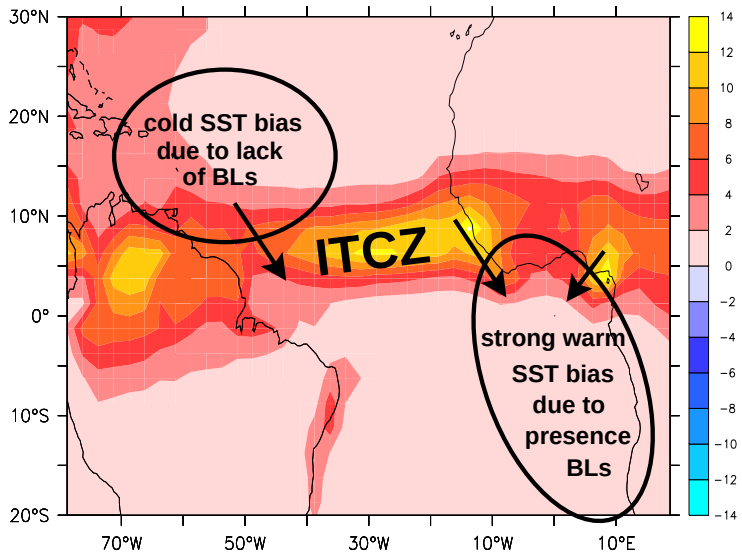

Figure 10: Illustration of potential feedback mechanisms between BL dynamics and SST biases over the tropical Atlantic. Background colors show the precipitation (in mm/day) from CMAP observations for JJA. The arrows indicate the southeastward displacement of the ITCZ in the models.

river basin (figure 5), causing less fresh water discharge from the Amazon river. The reduced fresh water discharge will increase the surface salinity over the NwTA, making it difficult for BLs to form. We speculate that the cold SST bias and the displaced ITCZ over the NwTA may also trigger a positive Wind–Evaporation–SST (WES) feedback (Chang et al., 1997) that is shown to operate in the deep western tropical Atlantic (Chang et al., 2000) during boreal winter and spring (Breugem et al., 2007). This may further amplify the biases in BLs, SST and ITCZ position. These feedback mechanisms may be responsible for the difficulty of the models in maintaining a warm pool over the NwTA. As mentioned in the introduction, not only coupled GCMs, but also atmospheric GCMs with prescribed observed SST suffer from a too southerly position of the ITCZ (Biasutti et al., 2002). This suggests that the too southerly position of the ITCZ in the models can be partly attributed to purely atmospheric processes as well (e.g. convection).

The presence of spurious model BLs over the SeEA during boreal spring and summer prevents strong mixed–layer cooling by vertical entrainment and turbulent mixing. As a result, a warm SST bias develops, which keeps the ITCZ closer to the equator. The excessive precipitation over the SeEA creates a layer of fresh surface water. Meanwhile, the warm SST bias over the SeEA weakens the equatorial easterlies, resulting in a deepened thermocline in the east and subsurface warming. The combined effect of freshening at the surface and warming at the subsurface maintains the spurious BLs with strong temperature inversions, and contributes to the warm SST bias in the models.

Previous studies proposed several other causes for the strong warm SST bias over the

SeEA. DeWitt (2005) suggested that it originates primarily from the too weak equatorial trade winds. This causes a too deep thermocline and too weak upwelling in the east, both of which contribute to reduction in entrainment cooling, while the opposite holds for the western equatorial Atlantic. A similar explanation was given by Chang et al. (2007) for the warm SST bias over the ACT region in the NCAR-CCSM3 model (Collins et al., 2006). As mentioned earlier, because of the tight air–sea coupling in the trade–wind–cold–tongue system, cause and effect of the weak trade wind and warm SST biases are difficult to assess. Hazeleger & Haarsma (2005) demonstrated the sensitivity of the cold tongue SST to changes in the wind–induced vertical mixing scheme for the upper ocean. Increasing the efficiency of vertical mixing led to a reduction in the warm SST bias over the cold tongue region in their coupled model and improved the seasonal migration of the marine ITCZ. All these studies suggest that a Bjerknes–type of feedback (Bjerknes, 1969) between SST, equatorial easterlies and thermocline displacement plays an important role in maintaining the warm SST bias over the SeEA in coupled climate models. The present study confirms that this mechanism is at work, but further suggests that it operates in concert with other positive feedback mechanisms, such as the interaction between BLs, SST and ITCZ displacement. Targeted sensitivity simulations with coupled models are needed to further quantify the importance of these feedback mechanisms.

The misrepresentation of the feedback between marine stratus clouds and local SST (Philander et al., 1996) has also been proposed as a possible cause for the warm SST bias off the African coast in the South Atlantic. The BL-SST-ITCZ feedback possibly enhances the stratus-SST feedback in this area, as some models, such as CSIRO-Mk3.0 model, develop a BL with a strong temperature inversion along the African coast during boreal summer (figure 3).

9 Conclusions

Consistent with the recent study by Foltz & McPhaden (2007), this study shows that BLs can have an important influence on the SST over the Atlantic warm pool region by suppressing entrainment cooling. Coupled climate models underestimate the extent and frequency of occurrence of BLs over the NwTA during boreal fall and winter, which partly contributes to the cold SST bias over this area. The lack of BLs is likely related to the high SSS bias in this region, which may, at least partially, be attributed to the southeastward displaced ITCZ in the models, the resulting precipitation deficit over the Amazon basin and the reduced discharge of fresh water from the Amazon river.

Contrary to observations, the models generate spurious BLs over the SeEA during boreal spring and summer. These BLs tend to suppress the development of the Atlantic cold tongue in these seasons, resulting in a strong warm SST bias over this area. The formation of these BLs likely originates from the low SSS all year round and the development of a warm subsurface bias during boreal spring and summer. The low SSS is caused by the excessive precipitation over the ACT region associated with the southeastward displaced ITCZ during boreal spring and summer. The subsurface warm bias is probably caused by

the too weak equatorial trades, making the thermocline too shallow in the west and too deep in the east.

The formation of BLs in the tropical Atlantic involves potential positive ocean–atmosphere feedbacks. Over the NwTA, the cold SST bias causes the ITCZ to shift southeastward, reducing the precipitation in the region and over the Amazon basin. This leads to a high SSS bias over the NwTA, making it difficult for BLs to form and thus maintains the cold SST bias. Over the ACT region, a similar BL–SST–ITCZ feedback mechanism may be at work, which may act to amplify a Bjerknes–type feedback between SST, equatorial easterlies and thermocline displacement.

The success of coupled climate models in accurately simulating the tropical Atlantic climate depends critically on how well they capture the feedback mechanisms that are at work in this region. This study shows that the models fail to accurately represent the feedback between BLs, SST and ITCZ displacement. This failure may contribute significantly to the biases in the tropical Atlantic climate. Further modeling and observational studies are needed to test and quantify the importance of this climate feedback. If it is indeed important, then coupled climate models need to be improved for an accurate simulation of the upper ocean salinity field, since the formation of BLs depends critically on the vertical salinity stratification in the upper ocean.

Acknowledgments

We acknowledge the international modeling groups for providing their data for analysis, the Program for Climate Model Diagnosis and Intercomparison (PCMDI) for collecting and archiving the model data, the JSC/CLIVAR Working Group on Coupled Modeling (WGCM) and their Coupled Model Intercomparison Project (CMIP) and Climate Simulation Panel for organizing the model data analysis activity, and the IPCC WG1 TSU for technical support. The IPCC Data Archive at Lawrence Livermore National Laboratory is supported by the Office of Science, U.S. Department of Energy. The figures in this paper have been made with the free Ferret software developed by TMAP at NOAA/PMEL. WPB acknowledges the Netherlands Organization for Scientific Research (NWO) for financial support under the ALW-project 854.00.014. PC acknowledges the supports from the National Science Foundation (NSF) under the project OCE-0623364 and the National Oceanic and Atmospheric Administration (NOAA) under the project NA05OAR4311136.

Appendix A: Procedure for computing BL characteristics

For each month and at each grid point of the SODA reanalysis and the output of the models, the ILD and the MLD were computed based on the criteria given by equations (1) and (2), respectively. If the ILD exceeded the MLD by 10 m, then the layer in between the base of the ILD and MLD was considered as a 'true' BL, and its thickness was computed as

the difference ILD–MLD. A threshold of 10 m was chosen, because this corresponds to the typical vertical grid resolution near the ocean surface of both SODA and the models (see the square symbols in figure 1). When a true BL was detected, it was checked whether the vertical temperature profile contained a subsurface maximum inside the BL, and if so, the magnitude of the temperature inversion was computed as the difference between the maximum temperature and the temperature at 10 m depth. Next, the monthly climatologies were computed by averaging over all years in which a BL was detected. For example, the climatological mean BL thickness for January was computed by averaging over all years in which a BL was detected in January. Similarly, the frequency of BL occurrence in January was calculated by first assigning all Januaries in which a true BL was detected the value 1 and otherwise the value 0, and then by averaging over all these values.

The seasonal climatologies shown in figures 2 and 3 were obtained by averaging the monthly climatologies over the respective seasons. Because at some grid points a BL may be detected in a specific month, but possibly never in the preceding and/or the next month, the grid points of the monthly climatology fields without a value (i.e. where a BL was never detected) were first assigned the value 0 prior to the seasonal averaging.

References

[1] Biasutti, M., A. H. Sobel, & Kushnir, Y. 2006 AGCM precipitation biases in the tropical Atlantic. *J. Clim.* **19**, 935–958.

[2] Bjerknes, J. 1969 Atmospheric teleconnections from the equatorial Pacific. *Mon. Wea. Rev.* **97(3)**, 163–172.

[3] Breugem, W.-P., Hazeleger, W., & Haarsma, R. J. 2006 Multimodel study of tropical Atlantic variability and change. *Geoph. Res. Lett.* **33**, L23706, doi:10.1029/2006GL027831.

[4] Breugem, W.-P., Hazeleger, W., & Haarsma, R. J. 2007 Mechanisms of northern tropical Atlantic variability and response to CO_2 doubling. *J. Clim.* **20(11)**, 2691–2705.

[5] Carton, J. A., & Giese, B. S. 2007 SODA: a reanalysis of ocean climate. *Mon. Wea. Rev.*, in press.

[6] Chang, P., Ji, L., & Li, H. 1997 A decadal climate variation in the tropical Atlantic ocean from thermodynamic air–sea interactions. *Nature* **385**, 516–518.

[7] Chang, P., Saravanan, R., Ji, L., & Hegerl, G. C. 2000 The effect of local sea surface temperatures on atmospheric circulation over the tropical Atlantic sector. *J. Clim.* **13**, 2195–2216.

[8] Chang, C-Y, Carton, J. A., Grodsky, S. A., & Nigam, S. 2007 Seasonal Climate of the Tropical Atlantic Sector in the NCAR Community Climate System Model 3: Error Structure and Probable Causes of Errors. *J. Clim.* **20(6)**, 1053–1070.

[9] Collins, W. D., et al. 2006 The Community Climate System Model version 3 (CCSM3). *J. Clim.* **19(11)**, 2122–2143.

[10] Davey, M. K., et al. 2002 STOIC: a study of coupled model climatology and variability in tropical ocean regions. *Clim. Dyn.* **18**, 403–420.

[11] de Boyer Montégut, C., Mignot, J., Lazar, A., & Cravatte, S. 2007 Control of salinity on the mixed layer depth in the world ocean. Part I: General description. *J. Geoph. Res.* **112**, C06011, doi:10.1029/2006JC003953.

[12] DeWitt, D. G. 2005 Diagnosis of the tropical Atlantic near-equatorial SST bias in a directly coupled atmosphere-ocean general circulation model. *Geoph. Res. Lett.* **32**, L01703.

[13] Foltz, G. R., Grodsky, S. A., & Carton, J. A. 2003 Seasonal mixed layer heat budget of the tropical Atlantic ocean. *J. Geoph. Res.* **108(C5)**, 3146.

[14] Foltz, G. R., Grodsky, S. A., & Carton, J. A. 2004 Seasonal salt budget of the northwestern tropical Atlantic ocean along 38°W. *J. Geoph. Res.* **109**, C03052, doi:10.1029/2003JC002111.

[15] Foltz, G. R., & McPhaden, M. J. 2007 Impact of barrier layer thickness on the sea surface temperature of the tropical North Atlantic ocean. *Geoph. Res. Lett.*, submitted.

[16] Gill, A. E. 1982 Atmosphere-ocean dynamics. Academic Press, Inc., 662 pp.

[17] Godfrey, J. S., & Lindstrom, E. J. 1989 The heat budget of the equatorial western Pacific surface mixed layer. *J. Geoph. Res.* **94(C6)**, 8007–8017.

[18] Gordon, C., et al. 2000 The simulation of SST, sea ice extents and ocean heat transports in a version of the Hadley Centre coupled model without flux adjustments. *Clim. Dyn.* **16**, 147–168.

[19] Gordon, H. B., et al. 2002 The CSIRO Mk3 climate system model. *CSIRO Atmos. Res. Tech. Pap. No. 60*, 130 pp.

[20] Hazeleger, W., & Haarsma, R. J. 2005 Sensitivity of tropical Atlantic climate to mixing in a coupled ocean-atmosphere model. *Clim. Dyn.* **25**, 387–399.

[21] IPCC 2007. Climate change 2007: the physical science basis. Contribution of Working Group I to the fourth assessment report of the Intergovernmental Panel on Climate Change [Solomon, S., Qin, D., Manning, M., Chen, Z., Marquis, M., Averyt, K. B.,

Tignor, M., & Miller, H. L. (eds.)]. Cambridge University Press, Cambridge, United Kingdom and New York, NY, USA, 996 pp.

[22] Jochum, M., Murtugudde, R., Ferrari, R., & Malanotte-Rizzoli, P. 2005 The impact of horizontal resolution on the tropical heat budget in an Atlantic ocean model. *J. Clim.* **18(6)**, 841–851.

[23] Kraus, E. B., & Turner, J. S. 1967 A one–dimensional model of the seasonal thermocline. II. The general theory and its consequences. *Tellus* **XIX**, 98–105.

[24] Maes, C., Picaut, J., & Belamari, S. 2002 Salinity barrier layer and onset of El Niño in a Pacific coupled model. *Geoph. Res. Lett.* **29(24)**, 59.1–59.4.

[25] Masson, S., & Delecluse P. 2001 Influence of the Amazon river runoff on the tropical Atlantic. *Phys. Chem. Earth, part B* **26(2)**, 137–142.

[26] Mignot, J., de Boyer Montégut, C., Lazar, A., & Cravatte, S. 2007 Control of salinity on the mixed layer depth in the world ocean. Part II: tropical areas. *J. Geoph. Res.*, in press.

[27] Mitchell, T., & Wallace, J. M. 1992 The annual cycle in equatorial convection and sea surface temperature. *J. Clim.* **5**, 1140–1156.

[28] Murtugudde, R., & Busalacchi, A. J. 1998 Salinity effects in a tropical ocean model. *J. Geoph. Res.* **103(C2)**, 3283–3300.

[29] Okumura, Y., & Xie, S.-P. 2004 Interaction of the Atlantic equatorial cold tongue and the African monsoon. *J. Clim.* **17**, 3589–3602.

[30] Pailler, K., Bourlès, B, & Gouriou, Y. 1999 The barrier layer in the western tropical Atlantic Ocean. *Geoph. Res. Lett.* **26(14)**, 2069–2072.

[31] Peter, A.-C., et al. 2006 A model study of the seasonal mixed layer heat budget in the equatorial Atlantic. *J. Geoph. Res.* **111**, C06014, doi:10.1029/2005JC003157.

[32] Philander, S. G. H., & Pacanowski, R. C. 1981 The oceanic response to cross-equatorial winds (with application to coastal upwelling in low latitudes). *Tellus* **33**, 201–210.

[33] Philander, S. G. H., Gu, D., Lambert, G., Li, T., Halpern, D., Lau, N.-C., & Pacanowski, R. C. 1996 Why the ITCZ is mostly north of the equator. *J. Clim.* **9(12)**, 2958-2972.

[34] Salas-Mélia, D., et al. 2005 Description and validation of the CNRM-CM3 global coupled model. *Clim. Dyn.*, submitted.

[35] Sato, K., Suga, T., & Hanawa, K. 2006 Barrier layers in the subtropical gyres of the world's oceans. *Geoph. Res. Lett.* **33**, L08603, doi:10.1029/2005GL025631.

[36] Sprintall, J., & Tomczak, M. 1992 Evidence of the barrier layer in the surface layer of the tropics. *J. Geoph. Res.* **97(C5)**, 7305–7316.

[37] Stevenson, J. W., & Niiler, P. P. 1983 Upper ocean heat budget during the Hawaii-to-Tahiti shuttle experiment. *J. Phys. Ocean.* **13**, 1894–1907.

[38] Uppala, S. M., et al. 2005 The ERA-40 reanalysis. *Quart. J. Royal Meteorol. Soc.* **131(612)**, 2961–3012.

[39] Vialard, J., & Delecluse, P. 1998a An OGCM study for the TOGA decade. Part I: role of salinity in the physics of the western Pacific fresh pool. *J. Phys. Ocean.* **28**, 1071–1088.

[40] Vialard, J., & Delecluse, P. 1998b An OGCM study for the TOGA decade. Part II: barrier-layer formation and variability. *J. Phys. Ocean.* **28**, 1089–1106.

[41] Xie, P., & Arkin, P. A. 1997 Global precipitation: a 17-year monthly analysis based on gauge observations, satellite estimates, and numerical model outputs. *Bull. Amer. Meteor. Soc.* **78**, 2539–2558.

[42] Xie, S.-P. 2004 The shape of continents, air-sea interaction, and the rising branch of the Hadley circulation. In The Hadley Circulation: Past, Present and Future [Diaz, H. F., & Bradley, R. S. (eds.)]. Kluwer Academic Publishers, Dordrecht, 121–152.